Acta Crystallographica Section D
Biological Crystallography
ISSN 0907-4449

Structure of a monoclonal 2E8 Fab antibody fragment specific for the low-density lipoprotein-receptor binding region of apolipoprotein E refined at 1.9 Å

Sergei Trakhanov,[a,b,c] Sean Parkin,[c] Robert Raffaï,[a,b,d] Ross Milne,[d] Yvonne M. Newhouse,[a] Karl H. Weisgraber[a,b,e] and Bernhard Rupp[c]*

[a]Gladstone Institute of Cardiovascular Disease, University of California, San Francisco, CA 94141, USA, [b]Cardiovascular Research Institute, University of California, San Francisco, CA 94141, USA, [c]Biology and Biotechnology Research Program, Lawrence Livermore National Laboratory, Livermore, CA 94551, USA, [d]Lipoprotein and Atherosclerosis Group, University of Ottawa Heart Institute and Department of Pathology and Biochemistry, University of Ottawa, Ontario, K1Y 4E9, Canada, and [e]Department of Pathology, University of California, San Francisco, CA 94141, USA

Correspondence e-mail: br@llnl.gov

Received 23 March 1998
Accepted 9 July 1998

PDB Reference: 2E8 Fab antibody fragment, 12e8.

The crystal structure of the Fab fragment of 2E8, the monoclonal IgG1,κ antibody specific for the low-density lipoprotein (LDL) receptor-binding region of apolipoprotein E (apoE), has been solved by molecular replacement and refined at 1.9 Å resolution (PDB entry 12E8). Two 2E8 Fab molecules in the asymmetric unit are related by noncrystallographic symmetry and are hydrogen bonded through a β-sheet-like intermolecular contact between the heavy-chain complementarity-determining regions 3 (CDRH3) of each molecule. The structure has been refined to an R value of 0.22 ($R_{\rm free}$ = 0.27). The initially ill-defined heavy-chain constant domain (C_{H1}) of 2E8 has been retraced with the aid of automatic refinement, confirming the β-sheet tracing independently of any starting models. As a resolution better than 2 Å is not common for Fab fragments, this model represents a well defined Fab structure and should prove useful in MR solution of other Fab fragments. Furthermore, in the absence of an LDL-receptor structure, the homology of the 2E8 CDRH2 to the ligand-binding domain of the LDL receptor has been exploited to model the apoE–LDL-receptor interaction.

1. Introduction

Apolipoprotein E (apoE, 34 kDa, 299 residues) is a protein component of several classes of human plasma lipoproteins (Mahley *et al.*, 1984; Mahley, 1988; Weisgraber, 1994). As a ligand for the low-density lipoprotein (LDL) receptor and other lipoprotein receptors in the LDL-receptor family, apoE plays a major role in modulating plasma lipoprotein metabolism. Variant forms of apoE, including apoE2, bind defectively to the LDL receptor and are an underlying cause of type III hyperlipoproteinemia, a disorder in lipid metabolism associated with premature heart disease (Mahley & Rall, 1995).

The structure of the apoE 22 kDa amino-terminal fragment (residues 1–191) containing the LDL-receptor binding region (residues 136–150) has been determined (Wilson *et al.*, 1991). The LDL-receptor binding region is characterized by a cluster of basic residues that are thought to interact with complementary clusters of acidic residues contained within the LDL-receptor ligand-binding domain (Mahley, 1988). Detailed structural information on the LDL receptor is not yet available, although structures of cysteine-rich repeats 1 and 2 of the ligand-binding domain have been determined individually by nuclear magnetic resonance (NMR; Daly, Djordjevic *et al.*, 1995; Daly, Scanlon *et al.*, 1995), and recently the structure of repeat 5 has been determined by X-ray crystallography (Fass *et al.*, 1997).

In the absence of complete structural information on the intact LDL-receptor binding domain, we sought an alternative

approach to model the receptor–ligand interaction. Two monoclonal antibodies, designated 1D7 and 2E8, are known to block the interaction of apoE with the LDL receptor by binding to epitopes within the receptor-binding region of apoE (Raffaï *et al.*, 1995). Sequence alignment of the primary structures of the six complementarity-determining regions (CDRs) of the 1D7 and 2E8 antibodies with the seven cysteine-rich repeats of the LDL receptor reveals similarity between the 2E8 heavy chain CDRH2 and repeat 5 of the LDL receptor. Deletion mutagenesis analysis suggested that this repeat is involved in the interaction of apoE with the LDL receptor (Russell *et al.*, 1989). Both 2E8 and the LDL receptor share a decreased affinity for apoE2, the isoform responsible for type III hyperlipoproteinemia (Mahley & Rall, 1995; Dong *et al.*, 1996). The 2E8 heavy chain CDRH2 contains two glutamic acid residues and aspartic acid, which mimic the interaction of apoE with the LDL receptor. Examination of that interaction should provide useful insights into the mechanism of apoE–LDL-receptor binding. As a first step, we present the three-dimensional structure of the 2E8 Fab fragment at 1.9 Å resolution and initial modeling studies.

2. Experimental methods

2.1. Preparation and purification of 2E8 Fab fragments

The 2E8 hybridoma was prepared as described (Raffaï *et al.*, 1995). The 2E8 IgG1,κ (Ig, immunoglobulin) was purified from ascites of hybridoma-bearing mice by affinity chromatography on Protein G Sepharose and digested with papain [IgG:papain, 100:1(*w*/*w*)] for 6 h at 310 K. Undigested IgG and Fc fragments were removed by passage through a Protein A Sepharose column. The flow-through was dialyzed against 50 m*M* Tris pH 8.5, and applied to a pre-equilibrated column of DEAE Sephacel. The Fab fragments were finally eluted with a linear gradient of 0–0.1 *M* NaCl.

2.2. Crystallization

Crystals were grown at room temperature by the hanging-drop vapor-diffusion method in Linbro plates with 4 µl droplets [2 µl of protein solution (4 mg ml^{-1}) mixed with 2 µl of reagent] using well solutions from the Crystal Screen Macromolecular Crystallization Kit I (Hampton Research, Laguna Hills, CA). The most promising results were obtained with reagent #9, and the conditions were further optimized to 23%(*w*/*v*) polyethylene glycol (PEG) 4000, 0.10 *M* sodium citrate and 0.2 *M* ammonium acetate (pH 5.6). Crystals of dimensions 0.2 × 0.2 × 0.5 mm were obtained in 4–6 weeks.

2.3. Data collection

Diffraction data were collected on ADSC multiwire area detectors using graphite-monochromated Cu $K\alpha$ radiation from a Rigaku RU200 rotating-anode generator. The crystals were cryo-protected by equilibration for 2 min in mother liquor with an increased PEG concentration of 35%(*w*/*v*). The soaked crystals were quenched in liquid nitrogen and transferred with cryo-tongs into the nitrogen stream of a modified Siemens LT-2 low-temperature apparatus.[1] Data were collected at 125 K from two crystals (Table 1).

Table 1
Data-collection statistics for 2E8 Fab antibody fragment.

Temperature (K)	125
Space group	$P2_1$
a (Å)	66.69
b (Å)	65.55
c (Å)	103.39
β (°)	97.13
$d_{\rm min}$† (Å)	1.85
Number of observations	237795
Number of unique reflection	63078
Completeness (%)	84
$R_{\rm merge}$‡(%)	8.5
$\langle I/\sigma(I)\rangle$	6.0
Last shell used in refinement (Å)	2.02–1.90
Number of observations (last shell)	18169
Number of unique reflections (last shell)	8652
Completeness (last shell) (%)	77
$R_{\rm merge}$ (last shell)‡ (%)	22.7
$\langle I/\sigma(I)\rangle$ (last shell)	2.1

3. Structure solution and refinement of 2E8 Fab fragment

The structure of 2E8 Fab was solved by molecular replacement (MR) using murine Fab (PDB entry 6FAB, murine anti-*p*-azophenylarsonate Fab 36–71; Strong *et al.*, 1991) as a search model. 6FAB was choosen on the basis of sequence similarity (79 and 77% for the light and heavy chains, respectively) and resolution (1.85 Å). The length of the CDRs matches the loop length in the 2E8 Fab fragment, with the sole exception of 2E8 CDRH3, which is shorter by one residue. An alternate truncated molecular probe differing from 2E8 by only four residues was created from the constant domains of the light and heavy chains of the murine Fab (C_L and C_{H1}, residues from 107 to 214 and from 110 to 214 for C_L and C_{H1}, respectively). Residue numbering for 2E8 follows the Kabat nomenclature as assigned with program *KABATMAN* (Martin, 1996).

X-PLOR 3.1 (Brünger, 1992) was used for MR searches in variable resolution ranges, typically 15–5.0 Å or 10–4.0 Å. Patterson vectors from 5.0 to 30.0 Å were chosen for the rotation search, yielding an unambiguous solution (6σ peak) for both search models. Final rotation angles were obtained by Patterson correlation refinement (Brünger, 1992).

A second rotation solution was not found in the cross-rotation search, and a self-rotation search did not reveal a set of angles different from those determined by the crystallographic symmetry. We therefore concluded that the orientation of the noncrystallographic axis must be nearly parallel to the crystallographic twofold screw axis. A native Patterson map (Fig. 1) revealed a distinct peak in the Harker section, confirming the presence of a noncrystallographic symmetry (NCS) axis parallel to b near $x = 0.21$ and $z = 0.01$. The first

[1] Supplementary information about equipment and cryo-procedures used can be found at the WWW address http://www-structure.llnl.gov.

molecule was therefore rotated by 180° around *b* to obtain the orientation of the second molecule in the asymmetric unit. A translational search in the *XZ* plane using data from 6.0 to 3.0 Å yielded a clear solution (10σ above the mean) for the first molecule, which was fixed in its new position. A subsequent translational search using the second molecule gave a solution at 8σ above the mean.

After the MR solution, three steps of rigid-body refinement were applied. First, the two Fab fragments were treated as independent rigid bodies, followed by individual refinement of the light and heavy chains of each fragment. Finally, the variable and constant domains of both fragments were allowed to adjust their positions (eight domains in total, R = 45%). After the rigid-body refinement, the R value dropped to 40% (resolution shell 6.0–3.0 Å). The model was then subjected to 300 cycles of conjugate-gradient minimization in *X-PLOR* to arrive at R = 33% (6.0–2.5 Å).

The search model was converted to 2E8 by substitution of amino acids using *CHAIN* (Sack, 1988; Sack & Quiocho, 1997). The 2E8 model was then subjected to energy minimization, and the resolution extended stepwise to 1.95 Å. Subsequent simulated-annealing refinement (3000–300 K) followed by *B*-factor refinement reduced the R value to 27%. Initial electron-density $2F_o - F_c$ maps showed reasonable tracings within the β-sandwich core for each Ig domain of the model. The loop regions, including those constituting CDR regions, however, were not well defined.

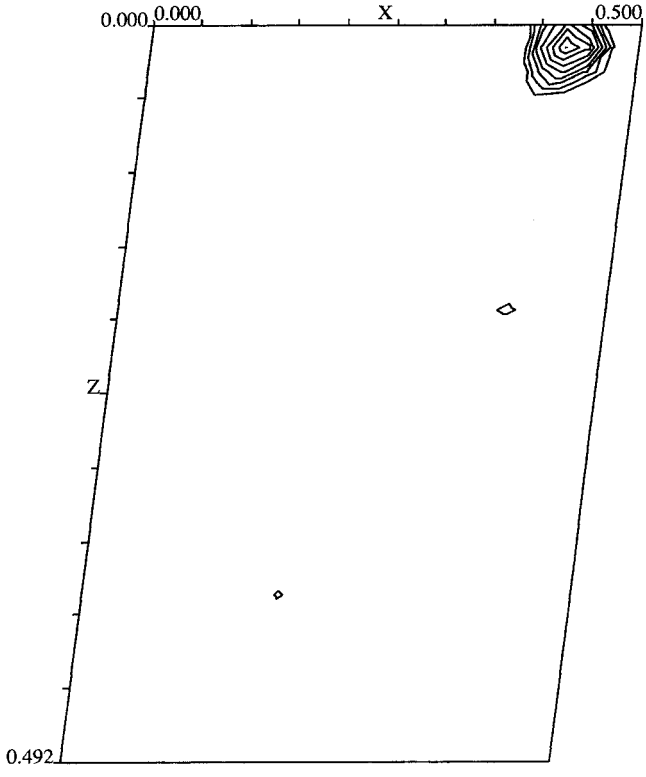

Figure 1
Native Patterson map created by *XtalView* (McRee, 1992) showing the strong Harker peak indicative of an NCS axis parallel to the crystallographic 2_1 screw axis.

Table 2
X-PLOR 3.851 refinement statistics.

Number of protein atoms	6662
Number of solvent atoms	767
Resolution range (Å)	20–1.90
Number of reflections in refinement	58785
Sigma cutoff	None
R value (%)	22.1
R_{free} (%)†	27.1
R.m.s. deviation in bond lengths (Å)	0.011
R.m.s. deviation in bond angles (°)	1.6
R.m.s. deviation in dihedral angles (°)	28.4
R.m.s. deviation in improper angles (°)	1.6

† The R_{free} value was calculated *a posteriori* (Brünger, 1997) for a 2% random set with the model coordinates subjected to simulated annealing to remove the memory of the test set. Details of the NCS setup are described in PDB entry 12e8.

To eliminate the ambiguous tracing of the loops, we replaced the bulk of the model with elements from an Fab fragment complexed with fluorescein (PDB entry 1FLR; Whitlow *et al.*, 1995) refined at 1.85 Å (R = 19%). From the initial 6FAB model, we retained the CDRL1 loop based on its good fit into electron density, and the C_{H1} domain because it is incomplete in the 1FLR model.

The new combined model was subjected to *de novo X-PLOR* refinement starting with rigid-body minimization. After corresponding amino-acid substitutions, simulated-annealing refinement and *B*-factor refinement the model yielded an R value of 22.5%. The $F_o - F_c$ and $2F_o - F_c$ omit maps demonstrated that five of the six CDR loops of the light and heavy chains of both molecules were fitted correctly. The 2E8 CDRH3 was completely different from 1FLR, however, and has been extensively rebuilt. In the final model-building step, the omitted residues of the switch regions were placed into electron density. The resulting model was iteratively rebuilt with *CHAIN* and refined with *X-PLOR*. The electron-

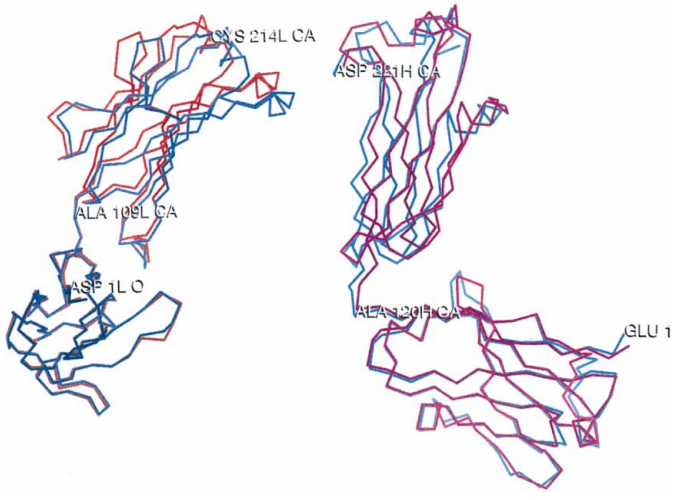

Figure 2
Superposition of NCS-related light chains (left) and heavy chains (right) on their respective variable domains, showing different angles in the switch region which required individual NCS setup for each of the four domains. The figure was created with *INSIGHT II*.

Table 3
Assignment of β-strands to corresponding domains of the light and heavy chains in 2E8.

Secondary structure was initially assigned with *DSSP* (Kabsch & Sanders, 1983) and verified by visual inspection of the refined 2E8 structure.

Domain	V_L	V_H	C_L	C_{H1}
Residues				
β-strand				
A	L1–L14	H2–H14	L111–L120	H117–H126
B	L17–L26	H16–H25	L129–L140	H136–H144
C	L32–L39	H32–H40	L143–L150	H149–H154
C′	L42–L50	H44–H53	—	—
C″	L61–L67	H55–H60	—	—
D	L69–L77	H66–H72	L158–L166	H163–H171
E	L83–L91	H76–H82B	L172–L182	H174–H183
F	L96–L105	H87–H96	L190–L198	H191–H201
G	—	H100B–H112	L204–L211	H204–H212

Table 4
Alignment of residues in LDL-receptor repeat 5 with complementarity-determining region 2 (CDRH2) of the 2E8 antibody.

Corresponding acidic residues are given in bold; additional acidic residues of LDL receptor are underlined.

195															210
LDL receptor															
Cys	Asp	Gly	Gly	Pro	**Asp**	Cys	Lys	**Asp**	Lys	Ser	**Asp**	Glu	**Glu**	Asn	Cys
2E8 CDRH2															
			Trp	Ile	**Asp**	Pro		**Glu**	Ile	Gly	**Asp**	Thr	**Glu**	Tyr	Val
			50	51	52	52A		53	54	55	56	57	58	59	60

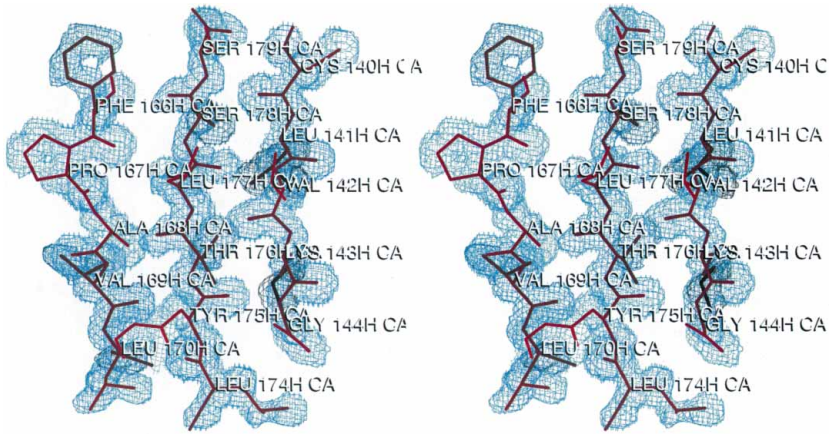

Figure 3
$2F_o - F_c$ electron-density map at 1σ level calculated after 90 cycles of *ARP* refinement and rebuilding. The electron density is superimposed with the *X-PLOR* model, demonstrating the correct tracing of β-strands (*B*, *D* and *E* displayed) of the 2E8 C_{H1} domain. The figure was created with *XtalView* (McRee, 1992).

density maps were calculated with the maximum-likelihood program of Urzhumtsev (1997).

At this stage in refinement, *X-PLOR 3.851* became available. Bulk-solvent modeling and all observed reflections including low-resolution data to 20 Å were used in a new refinement of the whole molecule. Inspection of the superimposed NCS-related heavy chains and light chains revealed different angles between the V and C domains for related chains, and individual NCS matrices had to be used for each of the four domains (Fig. 2). The switch regions connecting the variable and constant domains of either chain were not restrained by NCS. The most satisfying final model was obtained using the four individual NCS matrices applied to the β-strands of each domain, including C_{H1}. Refinement statistics are provided in Table 2 and in PDB entry 12E8 in which details of the NCS set up and the individual β-strand assignment used are described. All six CDR loops in the variable domains showed very well defined electron density,[2] but the loop connecting β-strands *A* and *B* in the C_{H1} domain (residues H128–H133) had very poor electron density in both molecules, and no reliable conformation could be established for this region.

4. Automatic refinement with *ARP*

In spite of the reasonable quality of the existing model (Table 2), the loop containing residues H128–H133 between the first and second β-strand in the C_{H1} domain of both Fab molecules was a concern. We attempted to improve the C_{H1} model by automatic refinement and model building with the program *ARP* (Lamzin & Wilson, 1993, 1997), and refinement with *REFMAC* (Murshudov *et al.*, 1997). New atoms added to the Fab structure according to comparison between $2F_o - F_c$ and $F_o - F_c$ electron-density maps were treated as O atoms with their van der Waals contact radii set to 1.2 Å in order to approximate the covalently bound atoms of a polypeptide chain.

At 1.9 Å, the data-to-parameter ratio of 1.9 for 2E8 was too low to use *ARP* successfully in unrestrained mode (*R* dropped to 18% but R_{free} increased to 37%). In restrained mode, two refinement schemes were applied using the full 2E8 model: (i) number of added water molecules matching the number of water molecules removed and (ii) one-step removal of a large number of atoms poorly fitted in the electron density followed by gradual rebuilding of the model by addition of new water molecules. For the last procedure, referred to as 'shock', the *ARP* authors recommend removing one quarter to one third of the model atoms (Lamzin & Wilson, 1997) before

[2] Images of omit maps of the CDRs are displayed at the WWW address http://www-structure.llnl.gov/fab/fab.htm.

rebuilding. No significant improvements of the poorly defined regions were achieved with either refinement scheme.

In an alternate approach, the C_{H1} domain and all associated solvent atoms were omitted from the model. The truncated model was subjected to simulated annealing in order to reduce model bias from previous refinement runs in the presence of the C_{H1} domain. The objective of this *ARP* rebuilding was not to achieve a low overall *R* value, but to obtain unbiased confirmation of the tracing in the C_{H1} domain. *ARP* was set up in restrained mode to add water molecules exceeding the number of removed water molecules by a factor of two to three in repeated cycles. Electron-density maps calculated after *ARP* refinement in the region of the omitted C_{H1} domain re-established most features of the omitted model. In particular, the correct tracing for β-strands (*B*–*E*) in the C_{H1} domain was evident (Fig. 3), but the maps were neither continuous nor showed enough contrast to allow unambiguous tracing of the *A*–*B* connecting loop.

5. Results and discussion

The 2E8 Fab antibody fragment (PDB entry 12E8) exhibits the typical immunoglobulin fold consisting of a heavy and a light chain, each containing a constant domain (C_L and C_{H1} for the light and heavy chain, respectively) and a variable domain (V_L and V_H). Three complementarity-determining regions in each of the two variable domains form the antigen-binding site. Fig. 4 presents a topological overview of the 2E8 Fab structure, including the second molecule related by non-crystallographic symmetry. The two Fab molecules interact through their V_H CDR regions with a short intermolecular antiparallel β-sheet arrangement formed between the CDRH3s of each molecule (Figs. 5 and 6). CDRH3 has the most conformational variability of the six CDR loops (Wilson & Stanfield, 1994). In contrast to 2E8, the NCS-related molecules in the anti-dsDNA Fab structure (Mol *et al.*, 1994) are in contact through their C_{H1} domains. The CDRs are of course involved in intermolecular contacts in anti-idiotope Fab–Fab complexes, but the details of their inter-Fab hydrogen bonding vary significantly (Evans *et al.*, 1994; Bentley *et al.*, 1990; Ban *et al.*, 1996). The head-to-head packing of the NCS-related molecules in the 2E8 structure also precludes the frequently observed head-to-tail packing in other Fab structures (Cygler *et al.*, 1987, and references therein).

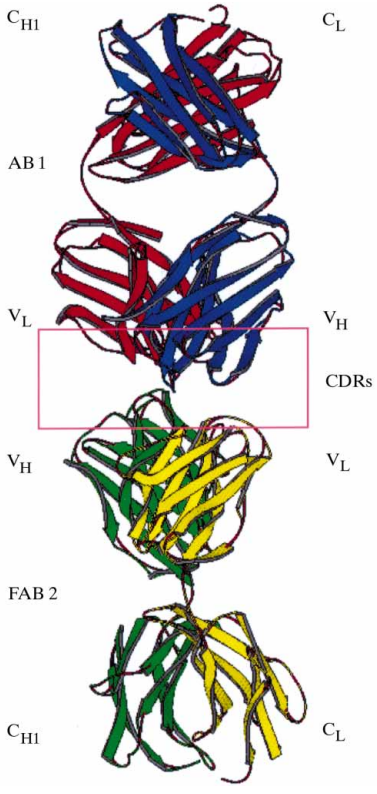

Figure 4
Ribbon representation of the topology of the 2E8 Fab dimer. The two light chains (C_L and V_L) are red and yellow, respectively, and the two heavy chains (C_{H1} and V_H) are blue and green, respectively. The dimer interface is formed by the complementarity-determining regions. The figure was created with *MOLSCRIPT* (Kraulis, 1991).

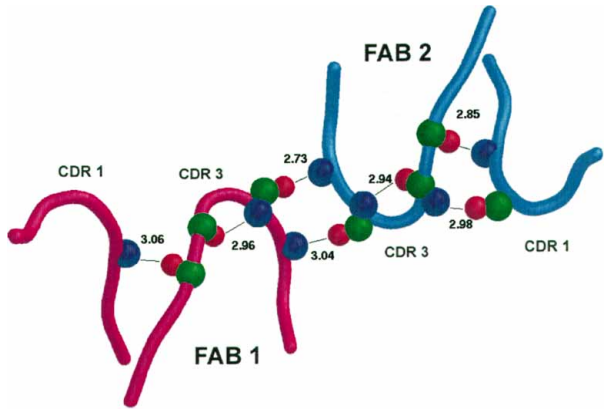

Figure 5
Intermolecular contacts between NCS-related Fab molecules. FAB 1, in magenta, is shown making extended β-sheet hydrogen-bonding contacts with its non-crystallographic pair FAB 2 in cyan. Two of the CDR loops from each molecule are involved in the extended sheet. The backbone trace for these CDRs are shown as tubes, carbonyl O atoms involved in hydrogen bonding are shown as CPK red spheres, carbonyl C atoms bound to displayed O atoms are shown as CPK green spheres and backbone N atoms involved in hydrogen bonding are shown as CPK blue spheres. Black lines represent hydrogen bonds, and bonding distances are indicated. This figure was generated with *MOLSCRIPT* (Kraulis, 1991).

The electron density is well defined throughout the majority of the 2E8 molecule.[3] Exceptions are the extreme carboxyl- and amino-terminal residues (approximately two to three residues) for both chains in each fragment, and the loop (residues H128–H133) connecting β-strands *A* and *B* in the C_{H1} domain (Table 3). Both situations are not uncommon in Fab models. In particular, the same regions of the C_{H1} domain are poorly defined in most Fab structures, and several authors have reported the complete absence of electron density for the corresponding region of their structures (Whitlow *et al.*, 1995; Barbas *et al.*, 1997, and references therein).

[3] Images of electron-density maps are displayed at the WWW address http://www-structure.llnl.gov/fab/fab.htm.

Several explanations for the lack of reliable tracing in parts of the C_{H1} domain of the Fab molecule are conceivable. Close similarity between all four domains in Fab molecules could create ambiguities during a molecular-replacement search similar to those reported recently in the case of an immunoglobulin light-chain dimer (Huang *et al.*, 1996). Neither the reasonably low R_{free} values nor the large number of agreeing independent structure solutions support this possibility. Poor tracing of this part of the C_{H1} domain probably results from dynamic or static disorder in this particular loop (Banfield *et al.*, 1996), or possible rearrangement of S—S bridges within the C_{H1} domain (Whitlow *et al.*, 1995). In our 2E8 structure, the region of the molecule containing the loop borders a solvent channel. Any intermolecular contacts that could stabilize a defined conformation are thus absent.

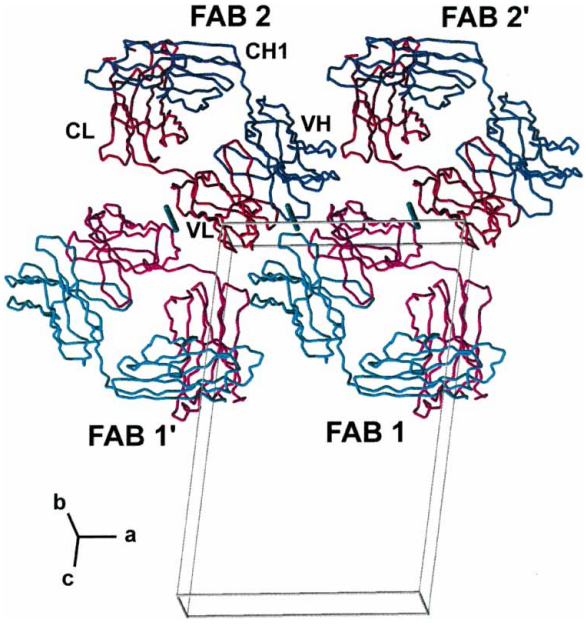

Figure 6
Molecular packing and non-crystallographic symmetry in the 2E8 crystal. FAB 1, shown with the light-chain Cα trace in magenta and the heavy chain in cyan, is related to FAB 2 (light chain shown in red and heavy chain in blue) by a twofold non-crystallographic symmetry axis located between CDRH3 of each molecule. Translation of FAB 1 by one unit-cell length in the negative *a* direction generates a second NCS axis relating FAB 1′ and FAB 2. Similarly, FAB 2′, generated by translation of FAB 2 by one unit-cell length in the positive *a* direction, is related to FAB 1 by NCS. Each of the NCS axes are shown in light green. This figure was generated using *MIDAS*.

The stereochemical quality of our final refined model was assessed with *PROCHECK* (Laskowski *et al.*, 1993) and *WHAT-CHECK* (Hooft *et al.*, 1996) showing that 88.4% of the residues fall in the most favored regions on a Ramachandran plot, 11.1% into additional allowed regions and only disordered residues Ala51 L(M) and Arg213 H(P) at the extreme of the carboxy-terminal of the heavy chains border disallowed regions. All six main-chain and five side-chain parameters describing model quality are better or comparable with the average set of parameters for structures determined at similar resolution.

6. LDL-receptor modeling

The sequence alignment of the heavy chain CDRH2 and repeat 5 of the LDL receptor with respect to the positions of acidic residues is shown in Table 4. It has been suggested that the acidic residues in the cysteine-rich repeats of the LDL receptor bind *via* an ionic interaction with the basic amino acids contained in the receptor-binding region of apoE (residues 136–150) (Mahley, 1988). Previous studies in which various repeats were deleted from the LDL receptor suggested that repeat 5 was particularly important for the interaction of the receptor with apoE, although other repeats in combination with repeat 5 were required for high-affinity binding (K_d = 2.8 n*M*; Russell *et al.*, 1989; Pitas *et al.*, 1979).

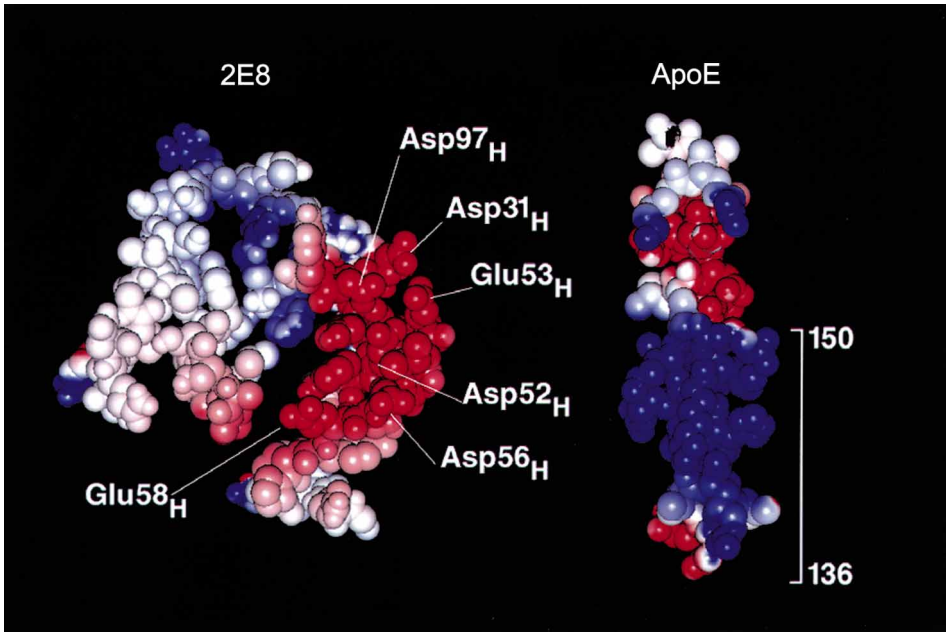

Figure 7
Electrostatic potential map of the solvent-accessible surface of the 2E8 CDRs and the receptor-binding region (residues 136–150) of apoE. Maps were calculated using *DELPHI* and displayed with *INSIGHT II*: red indicates negative potential, blue positive potential and white neutral.

The sequence similarity of the 2E8 CDRH2 with the LDL-receptor repeats and the reduced binding affinity of both 2E8 and the LDL receptor for apoE2 indicate that both molecules bind to to apoE by a similar mechanism. Moreover, we have recently observed a twofold increase in the affinity (K_d = 25 n*M*; Raffaï *et al.*, 1995) of a 2E8 variant in which Thr58 is replaced by a glutamic acid in CDRH2 (data not shown). In addition to increasing the content of acidic residues in CDRH2, this substitution also

increases its similarity to cysteine-rich repeat 5 of the LDL receptor. An additional parallel of 2E8 with the LDL receptor was revealed by examining the surface-accessible charge of the 2E8 CDRs. Calculation of the electrostatic potential map defined by the surface of the six CDRs demonstrated the presence of a large negative patch formed primarily by the four acidic residues in CDRH2 (Asp52, Asp56, Glu53 and Glu58; Fig. 7, left). In addition, Asp97 and Asp31 in the heavy chain CDR3 and CDR1, respectively, were in close proximity and contributed to the negative charge density. This negative patch occupies a major portion of the surface area defined by the six CDRs, and is similar in size and shape to the positive patch formed by residues 136–160 in apoE (Fig. 7, right). The similarity in complementary charged areas indicates that, to a large extent, the binding of 2E8 and apoE is mediated by electrostatic interactions, as is thought to be the case for the LDL receptor. The contribution to the negative patch of acidic residues from two other CDRs also parallels the interaction of multiple cysteine-rich repeats in the LDL receptor with apoE (Russell *et al.*, 1989).

In summary, the interaction of the 2E8 antibody with apoE mirrors the interaction of the LDL receptor with apoE. Identical regions on the apoE molecule are involved, and both interactions are similarly affected by substitutions within the receptor-binding domain as well as outside at position 158 (apoE2). Thus, in the absence of structural details on the intact ligand-binding domain of the LDL receptor, the interaction of 2E8 with apoE appears to be a useful model of this interaction. Studies to dock the 2E8 fragment and apoE3 and to determine the binding characteristics of 2E8 variants generated by *in vitro* mutagenesis, and attempts to obtain crystals of the 2E8–ApoE complex, are currently in progress.

The authors thank Bingyi Han for technical assistance, K. Humphrey for manuscript preparation, J. C. W. Carroll, B. Clark, S. Gonzales and A. Corder for graphic arts and G. Howard and S. Ordway for editorial assistance. Brent Segelke provided figures and a critical review of the manuscript. This work was supported by National Institutes of Health Program Project Grant HL41633 and by the United States Department of Energy at Lawrence Livermore National Laboratory under contract W-7405-Eng-48. The work was also supported by Grant T3142 from the Heart and Stroke Foundation of Ontario, and a studentship from the Heart and Stroke Foundation of Canada and from the Fonds pour la Formation de Chercheurs et l'Aide à la Recherche to RR.

References

Ban, N., Day, J., Wang, X., Ferrone, S. & McPherson, A. (1996). *J. Mol. Biol.* **255**, 617–627.
Banfield, M., King, D. J., Mountain, A. & Brady, R. L. (1996). *Acta Cryst.* D**52**, 1107–1113.
Barbas, C. F. III, Heine, A., Zhong, G., Hoffman, T., Gramatikova, S., Björnestedt, R., List, B., Anderson, J., Strua, E. A., Wilson, I. A. & Lerner, R. A. (1997). *Science*, **278**, 2085–2092.
Bentley, G. A., Boulot, G., Riottot, M. M. & Poljak, R. J. (1990). *Nature (London)*, **348**, 254–257.
Brünger, A. T. (1992). *X-PLOR*, Version 3.1. *A System for X-ray Crystallography and NMR.* New Haven: Yale University Press.
Brünger, A. T. (1997). *Methods Enzymol.* **277**, 366–396.
Cygler, M., Boodho, A., Lee, J. S. & Anderson, W. F. (1987). *J. Biol. Chem.* **262**, 643–648.
Daly, N. L., Djordjevic, J. T., Kroon, P. A. & Smith, R. (1995). *Biochemistry*, **34**, 14474–14481.
Daly, N. L., Scanlon, M. J., Djordjevic, J. T., Kroon, P. A. & Smith, R. (1995). *Proc. Natl Acad. Sci. USA*, **92**, 6334–6338.
Dong, L.-M., Parkin, S., Trakhanov, S. D., Rupp, B., Simmons, T., Arnold, K. S., Newhouse, M., Innerarity, T. L. & Weisgraber, K. H. (1996). *Nature Struct. Biol.* **3**, 718–722.
Evans, S. V., Rose, D. R., To, R., Young, N. M. & Bundle, D. R. (1994). *J. Mol. Biol.* **241**, 691–705.
Fass, D., Blacklow, S., Kim, P. S. & Berger, J. M. (1997). *Nature (London)*, **388**, 691–693.
Hooft, R. W. W., Vriend, G., Sander, C. & Abola, E. E. (1996). *Nature (London)*, **381**, 272–275.
Huang, D.-B., Ainsworth, C., Solomon, A. & Schiffer, M. (1996). *Acta Cryst.* D**52**, 1058–1066.
Kabsch, W. & Sanders, C. (1983). *Biopolymers*, **22**, 2577–2637.
Kraulis, P. J. (1991). *J. Appl. Cryst.* **24**, 946–950.
Lamzin, V. S. & Wilson, K. S. (1993). *Acta Cryst.* D**49**, 129–147.
Lamzin, V. S. & Wilson, K. S. (1997). *Methods Enzymol.* **277**, 269–305.
Laskowski, R. A., MacArthur, M. W., Moss, D. S. & Thornton, J. M. (1993). *J. Appl. Cryst.* **26**, 283–291.
McRee, D. E. (1992). *J. Mol. Graph.* **10**, 44–46.
Mahley, R. W. (1988). *Science*, **240**, 622–630.
Mahley, R. W., Innerarity, T. L., Rall, S. C. Jr & Weisgraber, K. H. (1984). *J. Lipid Res.* **25**, 1277–1294.
Mahley, R. W. & Rall, S. C. Jr (1995). In *The Metabolic and Molecular Bases of Inherited Disease*, 7th ed., edited by C. R. Scriver, A. L. Beaudet, W. S. Sly & D. Valle. New York: McGraw–Hill.
Martin, A. C. R. (1996). *Proteins Struct. Funct. Genet.* **25**, 130–133.
Mol, C. D., Muir, A. K. S., Lee, J. S. & Anderson, W. F. (1994). *J. Biol. Chem.* **269**, 3605–3614.
Murshudov, G. N., Vagin, A. A. & Dodson, E. J. (1997). *Acta Cryst.* D**53**, 240–255.
Pitas, R. E., Innererity, T. L., Arnold, K. S. & Mahley, R. W. (1979). *Proc. Natl Acad. Sci. USA*, **76**, 2311–2315.
Raffaï, R., Maurice, R., Weisgraber, K., Innerarity, T., Wang, X., MacKenzie, R., Hirama, T., Watson, D., Rassart, E. & Milne, R. (1995). *J. Lipid Res.* **36**, 1905–1918.
Russell, D. W., Brown, M. S. & Goldstein, J. L. (1989). *J. Biol. Chem.* **264**, 21682–21688.
Sack, J. S. (1988). *J. Mol. Graph.* **6**, 224–225.
Sack, J. S. & Quiocho, F. A. (1997). *Methods Enzymol.* **277**, 158–173.
Strong, R. K., Campbell, R., Rose, D. R., Petsko, G. A., Sharon, J. & Margolies, M. N. (1991). *Biochemistry*, **30**(15), 3739–3748.
Urzhumtsev, A. G. (1997). *Acta Cryst.* D**53**, 540–543.
Weisgraber, K. H. (1994). *Adv. Protein Chem.* **45**, 249–302.
Whitlow, M., Howard, A. J., Wood, J. F., Voss, E. W. Jr & Hardman, K. D. (1995). *Protein Eng.* **8**, 749–761.
Wilson, C., Wardell, M. R., Weisgraber, K. H., Mahley, R. W. & Agard, D. A. (1991). *Science*, **252**, 1817–1822.
Wilson, I. A. & Stanfield, R. L. (1994). *Curr. Opin. Struct. Biol.* **4**, 857–867.